The role of pH on the inhibition of aqueous zinc corrosion by L-tryptophan

N. Wint*, J.H. Sullivan, D. J. Penney

Materials Research Centre, College of Engineering, Swansea University, Bay Campus, Fabian Way, Crymlyn Burrow, Swansea, UK, SA1 8EN

Abstract: A combination of in situ Scanning Vibrating Electrode Technique (SVET), and time lapse photography were used to investigate the influence of the amino acid, L-tryptophan, on the localized corrosion occurring on unpolarized zinc (Zn) samples immersed in a 0.17 mol.L^{-1} aqueous sodium chloride electrolyte. The addition of 1 x 10^{-2} mol.L^{-1} of L-tryptophan was found to have a significant effect on the corrosion rate for all pH values tested. At both pH 2 and pH 7, primary protection was suggested to occur as a result of adsorption due to electrostatic interactions. A secondary mechanism, whereby an insoluble complex is formed between Zn (II) ions and anionic L-tryptophan, was also proposed to occur at areas of localized high pH. At pH 2 the additions resulted in an 88 % decrease in mass loss, as measured by gravimetric mass loss results and SVET, demonstrating the effectiveness of L-tryptophan inhibitors for this material.

*Corresponding author: Tel: +44 7376357305
E-mail address: n.wint@swansea.ac.uk

1. Introduction

Zinc (Zn) and Zn alloy galvanized steel is used heavily in the construction, automotive and domestic appliance manufacturing industries. The Zn layer on galvanized steel acts sacrificially and therefore provides cathodic protection to the iron substrate beneath.

Zn based coatings are often used in conjunction with chromate corrosion inhibitors, which are being phased out of use under Registration, Evaluation, Authorisation and Restriction of Chemicals (REACH) regulations. Current research for corrosion inhibitors is consequently focused on environmentally friendly 'green' alternatives and recent work has concentrated on the effect of various organic inhibitors on the corrosion of Zn and galvanized steel in neutral, weak acid and weak alkaline solutions [1-8].

Amino acids are non toxic and relatively cheap, soluble in aqueous solutions, and can be produced with high purity. These attributes make them suitable candidates for investigation as potential organic corrosion inhibitors on zinc [9]. The amino acid derivative, Tricine, has previously been associated with an inhibition efficiency of 90.3% during the study of the corrosion of pure zinc in a neutral sodium chloride (NaCl) electrolyte [10]. The inhibition was attributed to the physical adsorption of Tricine through the oxygen or nitrogen atoms on the active centres of the corroding surface [10]. L-tryptophan, the molecular structure of which is shown in Figure 1, is a non polar, aromatic amino acid and is of particular interest due to its molecular structure, within which the indole ring, nitrogen, and oxygen atoms are all possible active adsorption sites. It has been found to exhibit the best inhibition on Al at low pH, with respect to other amino acids during a study which also included alanine, leucine, valine, proline and methionine [11]. During this work its ability to suppress corrosion was attributed to the excess nitrogen atoms, the presence of an aromatic ring in the

molecule which can increase its adsorption to metallic substrates, and to its large molecular size that increases its coverage ability [11].

(Figure 1)

L-tryptophan has been shown to work effectively as an inhibitor to corrosion on both low carbon steel [12] and copper [13] in acidic conditions relevant to industrial acid cleaning, oil well acidification, and descaling.

However, it is well known that, in aqueous solutions, ionization of amino acids is pH dependent, and it is consequently of importance that the inhibitive effect of L-tryptophan is understood in electrolytes of varying pH. The zwitter ion structure of L-tryptophan is dominant in the range between pH 2.38 and pH 9.38 [14] due to the self protonation of the amine group from the carboxylic acid functional group. Below or above this pH range acid-base dissociation reactions, given by equation (1) and equation (2), occur and the molecules are cationic or anionic, respectively.

$$COO^- + H^+ \rightleftarrows COOH \qquad pKa_1 = 2.38 \qquad (1)$$

$$NH_3^+ \rightleftarrows NH_2 + H^+ \qquad pKa_2 = 9.39 \qquad (2)$$

Here, a combination of in situ scanning vibrating electrode technique (SVET), time lapse photography, and surface characterization is employed to study the inhibitive effect of L-tryptophan on pure Zn, freely corroding in aqueous sodium chloride (NaCl) electrolyte of varying pH. It is believed that a fundamental understanding of the behaviour of L-tryptophan, used in conjunction with pure zinc, is vital to the understanding of more complex technologically important zinc based coatings. The SVET is non-perturbing and thus offers advantages over conventional electrochemical measurements as it provides

insight into the dynamic changes in corrosion activity in the presence of the inhibitor, and subsequently offers scope to investigate the mechanism of inhibition [15]. The SVET has been used extensively to investigate the cut edge corrosion of Zn coated steels [16-19] and its ability to study the inhibitive effect of phosphates on the corrosion of magnesium [15] and zinc magnesium aluminium (ZMA) alloy coated steel has been shown previously [20].

2. Experimental

Materials: Zinc foil of 0.5 mm thickness and 99.95 % purity was obtained from Goodfellow Cambridge Ltd.

NaCl, L-tryptophan and all other chemicals were obtained from Sigma Aldrich Chemical Co. and were of analytical grade purity. A 0.17 $mol.L^{-1}$ (M) NaCl electrolyte was used throughout. L- tryptophan was added at concentrations of 1 x 10^{-2} M, 1 x 10^{-3} M and 1 x 10^{-4} M. Bulk solution pH was adjusted by the drop-wise addition of either HCl (aq) or NaOH (aq).

Methods: In the case of electrochemical characterization experiments, coupons of approximately 40 mm x 30 mm were cut from large sheets to obtain a suitably sized sample. Samples were ground to a European P-grade P1200 grit finish using silicon carbide (SiC) abrasive paper and were cleaned and degreased using ethanol and distilled water before experimentation. They were then masked using extruded Polytetrafluoroethylene (PTFE) tape (type 5490 HD supplied by 3 M) which exposed a 10 mm × 10 mm area in the centre. Electrochemical measurements were taken using a Solartron 1280 Electrochemical Measurement Unit at 25 °C**.** A saturated calomel electrode (SCE) reference electrode was used to provide a fixed potential throughout the experiment. For potentiodynamic polarization experiments, separate samples were polarized positively from OCP at a rate of

0.167 $mV.s^{-1}$ in the case of the anodic branch, and negatively from OCP in the case of the cathodic branch. Linear polarization resistance (LPR) experiments were carried out, whereby the working electrode was polarized 15 mV either side of the OCP at a rate of 0.167 $mV.s^{-1}$, and the polarization resistance (R_p) value was calculated from the slope of the potential-current lines. In both cases a platinum gauze counter electrode was employed. The R_p value calculated is inversely proportional to the corrosion rate and thus the inhibition efficiency was calculated using equation (3), where R_{p0} is the polarization resistance in the absence of L-tryptophan and R_{pi} is the polarization resistance in the presence of L-tryptophan.

$$\left[1 - \frac{R_{p0}}{R_{pi}}\right] x\ 100 \qquad (3)$$

Gravimetric mass loss experiments were carried out on 50 mm x 50 mm sized samples of thickness 0.5 mm. Coupons were cleaned and weighed. Samples were then fully immersed in the relevant electrolyte for a period of one week. Corrosion products were removed in saturated glycine (NH_2CH_2COOH) water solution at 20 °C following the International Organization for Standardization (ISO) 8407 standard, and the mass loss measured [21, 22].

SVET scans were performed to give insight into corrosion mechanism and relative corrosion performance. The SVET detects an alternating potential at the vibration frequency, which is proportional to the potential gradient in the direction of vibration.

Full details of SVET instrument design, mode of operation and calibration procedure to give values of current flux density along the axis of probe vibration (j_z), have been described elsewhere [23-26]. In short, the SVET consists of a glass encased 125 μm diameter platinum wire microtip which is vibrated, in the z direction, at a constant frequency (140 Hz), amplitude (25 μm) and height (100 μm) above the immersed corroding sample. At

this probe-to-sample distance it was believed that any interference from hydrogen bubbles, observed at low pH, would be minimised [15].

Samples were prepared in the same way as during electrochemical characterization studies. The SVET probe made 50 measurements along both the width and length of the sample, creating a mesh of 2500 data points. One scan was taken per hour for a period of 24 hours and tests were repeated three times in the case of each electrolyte. The dissolved oxygen and carbon dioxide concentrations in bulk solution were assumed to be 2.8×10^{-4} **M** and 1.32×10^{-5} **M** respectively, the equilibrium concentrations for air saturated water [27]. After 24 hours of immersion electrolyte pH was re-measured and any changes noted.

SVET data can be used semi quantitatively to estimate the total mass loss over time by determining time dependent total anodic current (Ia_t) and thus area averaged anodic current density (Ja_t) associated with each of the j_z distribution maps produced per scan according to equation (4)

$$Ia_t = A.Ja_t \geq \int_0^X \int_0^Y [\, j_{z(x,y)} > 0]\, dx\, dy \qquad (4)$$

where A is sample area and X and Y are the length and width of the SVET scan respectively. Numerical integration was carried out over the entirety of the exposed surface using the trapezium rule, allowing one Ia_t value to be obtained for each scan. From area averaged Ja_t current density values, the total equivalent mass loss could be calculated using Faraday's Law. The total quantity of charge emitted from the areas of local anodic activity over the duration of the experiments was calculated using equation (5)

$$Q = \frac{2F\ x\ mass\ loss}{65} = \int_{t=0}^{t=t_m} Ja_t dt \qquad (5)$$

where Q is the charge in $C.m^{-2}$, t_m is the immersion period in seconds, F is the Faraday

constant and mass loss is the total equivalent zinc loss (atomic weight 65 g) loss in $g.m^{-2}$ over period t. It is assumed that Ja_t remains constant between scans.

It should be considered that current density was measured 100 μm above the metal surface and thus the current detection efficiency was dependent on the local anode-cathode spacing [15]. Furthermore, although the mass loss data is semi quantitative due to the assumptions made during calculations, it is useful when making direct comparisons of mass loss in different electrolytes, and values obtained previously have been found to compare favourably with external weather Zn run off tests [28]. Good correlation between SVET derived corrosion inhibition efficiency values, and those obtained using methods such as EIS, mass loss determination and polarization curves have been noted previously [29].

In situ time lapse optical microscopy, which allowed the imaging of immersed corroding samples at a microstructural level, was employed following a methodology developed previously [20, 30]. In short, a polyethylene shroud was placed over the lens of a Meiji MT8000 microscope. A glass window in the shroud allowed the imaging of the sample surface whilst the lens was immersed in the electrolyte. Zinc samples, 20 mm x 20 mm in size, were mounted in phenolic resin and polished down to 1 μm. The surface was etched using 2 % Nital solution. PTFE tape (type 5490 HD supplied by 3 M) with a 1 mm diameter circle cut out was used to expose an area of 0.785 mm^2. The tape was also used to secure the sample to the bottom of a glass tank, which was subsequently filled with 250 ml of electrolyte. The microscope was then manoeuvred so as to image the exposed sample area. Images were captured every two minutes for a period of 24 hours using an infinity 2 camera attachment. Optical images acquired at pH 2 are not shown, firstly due to a general darkening of the surface in both the absence and the presence of L-tryptophan, and secondly due to the production of hydrogen bubbles which obscured the image.

SEM images showing surface morphology and microstructure were obtained using a Hitachi desktop microscope TM3000.

Samples for X-ray Phototelectron Spectroscopy (XPS) were sonicated in isopropanol and spectra were recorded on a Kratos Axis Supra instrument using an achromatic Al Kα source with an analysis area of 700 mm x 300 mm. Multiple high resolution analyses were recorded using a 0.1 eV step size with a pass energy of 20 eV and a 250 ms dwell time. To eliminate differential charging all samples were electronically floated and the integral charge neutraliser system used. CASA XPS software with Shirley backgrounds was used to charge correct the main C1s line to 284.8 eV and to calculate the areas of the C1s, O1s, N1s and Zn2p peaks.

3. Results

3.1 Electrochemical Characterization

The OCP of zinc in 0.17 M NaCl containing a range of L tryptophan concentrations was measured at 25 °C and are shown in Table 1 and in Figure 2. The confidence limits (errors) shown relate to one standard deviation on the mean, on the basis of three measurements.

(Table 1)

(Figure 2)

In the case of neutral electrolytes (Figure 2a), the sharp drop in potential for the highest inhibitor concentrations of 1×10^{-2} M and 1×10^{-3} M is indicative of a decrease in cathodic activity, or an increase in anodic activity. It should be noted that the time that elapses before this decrease in potential is greater for the highest concentration of 1×10^{-2} M. In the case

of the lowest L-tryptophan concentration of 1 x 10^{-4} M, the time dependent potential profile follows that obtained in the case 0.17 M NaCl with no addition. For electrolytes which contained 1 x 10^{-4} M and 1 x 10^{-3} M L-tryptophan, the final potential value is, within error, identical to that measured in the case of the control solution. The lower final potential value observed in the case of 1 x 10^{-2} M additions may suggest that the L-tryptophan is acting as a cathodic inhibitor. To further investigate the inhibitive effect of L-tryptophan in the case that pH<pKa_1, or pH>pKa_2 the experiments were repeated in electrolytes of varying bulk pH for the highest concentration of L-tryptophan. The behaviour observed at pH 11, Figure 2b, is similar to that discussed in the case of pH 7 electrolytes. In comparison, at pH 2, as shown in Figure 2c, the potential values obtained in the case of both the control electrolyte, and that containing the amino acid are, within error, identical which may be indicative of no effect on the corrosion behaviour of the Zn, or mixed inhibition. The potential value stabilises after a short duration indicating that any inhibitive effect occurs immediately.

Potentiodynamic curves obtained are shown in Figure 3a for pH 7 with different concentrations of L-tryptophan and Figure 3b and Figure 3c, both of which compare the control with inhibitor additions of 1 x 10^{-2} M, at pH 11 and pH 2 respectively. Differences in the cathodic branches of the polarization curves obtained at pH 7 (Figure 3a) and 11 (Figure 3b), to that obtained at pH 2 (Figure 3c) indicate that the zinc corrosion proceeds under cathodic control [31]. At pH 7 and 11, the OCP value is shifted more negatively in the presence of L-tryptophan. A current peak, centered at potentials of -1.09 vs. SHE, can be observed in the cathodic branch of the polarization curves. This value is consistent with the reduction of a $Zn(OH)_2$ film [32, 33]. This peak is absent in the case of the highest L-tryptophan concentration at pH 7 indicating that the L-tryptophan has modified the hydroxide covered surface. This suppression of the hydroxide reduction peak is not observed to the same

extent at pH 11. At pH 2 (Figure 3c) no cathodic shift in potential is observed for the L-tryptophan inhibited experiment and the curve appears similar to the control experiment. The cathodic branches of both curves display a degree of noise at this pH, indicative of H_2 gas formation. Examination of the currents associated with the cathodic and anodic branches for each pH value show similar current values for the 1 x 10^{-2} M inhibited and un-inhibited systems. However, the shift in OCP for the inhibited systems at pH 7 and pH 11, and the absence of the hydroxide reduction peak at the neutral pH, indicate that the inhibitor was interacting with the system. To explore this further, linear polarization experiments were subsequently completed with the aim of minimally perturbing the surface. The R_p values obtained after various times held at OCP are shown in Table 2, alongside the corresponding inhibition efficiency values calculated using equation (3). At pH 7 an inhibition efficiency of 78 % was initially achieved in the case of 1 x 10^{-2} M L-tryptophan additions. The calculated inhibition efficiency remained stable after the sample was left at OCP for 6 hours and increased to 83 % after 12 hours at OCP. In comparison, at pH 11, no inhibition was initially observed in the case of 1 x 10^{-2} M L-tryptophan additions. After the sample was held at OCP for 6 hours the inhibition efficiency increased to 25 %, and was 65 % after 12 hours at OCP.

(Figure 3)

(Table 2)

3.2 SVET and Time Lapse Microscopy Results

pH 7; The SVET derived surface plots of the normal current density above the freely corroding samples in pH 7 electrolytes, containing the range of L-tryptophan concentrations are shown in Figure 4. The plots shown were obtained after varying times

of electrolyte immersion, and were chosen to best represent the mechanistic differences observed at varying L-tryptophan concentrations. In the case of the control (Figure 4a and Figure 4b), corrosion is highly localized from the outset and the anode positions remain somewhat fixed with time once initiated, with peak anodic current densities of approximately 8 $A.m^{-2}$. Similarly, in the case of the lowest L-tryptophan concentration (Figure 4c and Figure 4d) corrosion is highly localized and initial sites of anodic activity can be seen all over the sample, as was the case for the control. At a concentration of 1 x 10^{-3} M a region of strong anodic activity is observed for the duration of the scan, as shown in Figure 4e and Figure 4f. This anodic region is surrounded by an area of low activity which expands with time. This process is illustrated using Figure 5 which shows a profile of the normal current density values, taken as a function of distance away from the focal anode (as shown by the arrow in Figure 5a) at 8 hour intervals. As time progress a ~30 % decrease in the anodic current density (arrow 1), and correspondingly, the adjacent cathodic current density (indicated by arrow 2) can be observed. These changes correspond with a ~1 mm extension of the region of low activity, indicated by arrow 3.

In comparison, in the case of the highest concentration of L-tryptophan, Figure 4g and Figure 4h, there is little evidence of significant activity up to 12 hours. After this point an anode can be observed for the remainder of the experiment, with peak current densities of around 1 $A.m^{-2}$. The time at which this occurs coincides with an almost twofold increase in the rate of mass loss from the sample, as calculated using SVET derived anodic j_z values (equation 4), and the drop in open circuit potential shown in Figure 2a. The total SVET derived mass loss for each inhibitor concentration is provided in Table 3 and these data demonstrate a 64% reduction in mass loss for an inhibitor concentration of 1 x 10^{-2} M. The

inefficiency of L-tryptophan as a corrosion inhibitor at the lower concentrations is shown in Table 3, with levels of mass loss similar to the control experiment, within error.

A further experiment was initiated, whereby 1 x 10^{-2} M L-tryptophan was introduced into the 0.17 M NaCl electrolyte after corrosion had been initiated. A twofold decrease in the rate of SVET measured mass loss, correlating with a drop in potential, was observed, demonstrating a decrease in cathodic current.

(Figure 4)

(Figure 5)

(Table 3)

The SVET results are supported by optical time lapse images shown in Figure 6. Figure 6a shows the surface of the zinc at one hour intervals during in situ immersion in pH 7 0.17 M NaCl. A number of anodic features, an example of which is labelled in the Figure 6a, initiate over the sample surface, some remaining stationary for the duration of the experiment, similar to the anodic peaks observed in the SVET experiment. Rings of corrosion product, previously suggested to form at the boundary of ionic counter currents from the anodic and cathodic regions, are also apparent [20]. The addition of the L-tryptophan alters the observed corrosion behaviour, as shown in Figure 6b. A uniform darkening of the surface is witnessed from the outset. In the final images (5-6 hours after immersion) an internal dark ring can be seen. This ring is again attributable to the formation of corrosion product and is similar to those observed previously when studying the corrosion of Zn-Mg-Al alloy coatings under the same technique and experimental conditions [20]. The formation

of corrosion product rings therefore indicates the establishment of corrosion on the sample surface and a breakdown of the inhibition afforded by the L-tryptophan.

(Figure 6)

The presence of an L-tryptophan based 'film' on the zinc surface is confirmed by the XPS data shown in Figure 7, for which the signal from scattered background electrons has been removed. A distinct peak, consistent with the presence of L-tryptophan, can be observed in the high resolution N1s spectra obtained from a sample immersed in 0.17 M NaCl with 1 x 10^{-2} M L-tryptophan additions. In the case that L-tryptophan was absent, no peak was observed. The relative atomic concentration of N, calculated by XPS, was (1.3 ± 0.3) at %. The confidence limits (errors) shown relate to one standard deviation, on the mean, on the basis of six measurements. Subsequently, since the atomic concentration of N in the L-tryptophan molecule is 13.3 %, it can be calculated that L-tryptophan corresponds to 11 % of the surface volume. This is consistent with approximately one monolayer of coverage, when assuming a sample depth of approximately 10 nm, and the molecule length of L-tryptophan to be 1.2 nm.

(Figure 7)

pH 11; To further investigate the inhibitive effect of L-tryptophan in the case that pH>pKa_2 the bulk electrolyte pH was increased to 11, and further SVET and time-lapse experiments carried out in the control NaCl electrolyte, and that containing the highest concentration of the L-tryptophan. In the control SVET experiment regions of anodic activity were observed to migrate across the surface of the sample over the first 12 hours of the experiment (Figure 8a and Figure 8b), in contrast to the focal anodes observed at pH 7. It is suggested that this change in mechanism from pH 7 to pH 11 is due to the increased thermodynamic likelihood

of precipitation of an insoluble corrosion product, which results in the relocation of the anodic and cathodic sites. At pH 11 the formation of an insoluble corrosion product such as zinc hydroxoxychlorides is entirely plausible [31, 34-35]. After 12 hours the anode had swept across the entire surface and thus remained fixed at this position for the remainder of the scan.

In the case that 1 x 10^{-2} M L-tryptophan is present, a single anode was initially observed in Figure 8c, the adjacent area being cathodic. After 8 hours of immersion, Figure 8d, little activity is observed, this being the case for the remainder of the experiment. This correlates with a decrease in corrosion potential shown in Figure 2b, and is indicative of a decrease in cathodic activity.

(Figure 8)

This finding is supported by time-lapse images in Figure 9a and Figure 9b, which show the surface of the zinc at 30 minute intervals during immersion in pH 11 0.17 M NaCl without and with added 1 x 10^{-2} M L-tryptophan. In the case of the former an initial area of anodic activity initiates in the first 60 minutes in the upper left quadrant of the exposed area, and a ring of corrosion product associated with the anode is precipitated readily at some distance from the site of metal dissolution. The anodic activity is then observed to progress towards the centre of the exposed sample, as indicated, with new corrosion product rings forming with time as the location of the anodic and cathodic activity move over the sample. Close examination of the individual images from the time lapse experiments show that the corrosion product rings that were initially formed display signs of dissolution as the anodic front progressed towards them, this being indicative of a local decrease in pH resulting from metal dissolution [20]. This progression of the anodic and cathodic activity over the

sample surface supports the observation from the SVET experiments and is somewhat different to the control time-lapse experiment at pH 7, where the anode and corrosion product rings were more sessile. In comparison, in the presence of 1 x 10^{-2} M L-tryptophan, shown in Figure 9b, there is a radical change in the mechanism in comparison to the pH 11 control. In Figure 9b (1) an anode initiated in the first 30 minutes in the lower right quadrant of the specimen, with a corrosion product ring developing. Over the next 30 minutes rapid darkening of the surface occurs local to the anodic regions, suggesting that inhibition is not complete and that the anodic activity still persists to some degree in this region, and progresses across the surface. In comparison to the uniform blackening, observed in the case of pH 7 electrolytes (Figure 6b), the remainder of the surface remains unchanged.

(Figure 9)

A comparison of the SVET measured mass loss for the samples immersed in 0.17 M NaCl and 0.17 M NaCl with 1 x 10^{-2} M L-tryptophan additions for pH 2, 7 and 11 is given in Table 4, which shows that an increased inhibitor efficiency of 80% is achieved at pH 11 when compared to that at pH 7 of 64%.

(Table 4)

pH 2; The SVET derived surface plots of the normal current density above the freely corroding samples in pH 2 0.17 M NaCl without (a and b) and with (c and d) 1 x 10^{-2} M L-tryptophan are shown in Figure 10. For the sample without inhibitor, from the time of immersion, the anodic area is distributed more generally across the entire surface throughout the 24 hour period. In comparison, the positive normal current density values observed in the presence of 1 x 10^{-2} M L-tryptophan, are considerably reduced suggesting that the L-tryptophan has a significant inhibitive effect on corrosion at this pH, with a

345 reduction in mass loss of 88 % (Table 4).

346 At this pH hydrogen can be formed as a product of the cathodic reaction [31]. The presence
347 of large H_2 bubbles on the SVET tip may cause the measurement of conspicuously distorted
348 signals and can lead to complete failure of measurements. This occurs very infrequently
349 when the tip is in motion as is the case during scanning. The lifetime of bubbles was short
350 in relation to scan time and repeat experiments showed that the effects due to the large
351 bubbles were negligible as found previously [15]. It was suggested that the potential error in
352 SVET measurements derived from displacement of electrolyte by H_2 bubbles was small.
353 An error of less than 10 %, this being of a similar order to the random error associated with
354 SVET measurements, was estimated [15].

355 ***(Figure 10)***

356 To confirm the validity of SVET derived mass loss values, physical mass loss
357 measurements, shown in Table 5, were recorded. This was felt necessary due to the more
358 generalized nature of corrosion observed on the control sample in the case of immersion in
359 pH 2 electrolyte. At this point it should be remembered that SVET mass loss estimates are
360 derived solely from localized corrosion where anodes and cathodes has a physical
361 separation greater that approximately 1.5 times the SVET tip scan height and therefore the
362 contribution from general corrosion may not be accounted for [15]. The mass loss was
363 calculated after one week of immersion, and the measured values are given in the third
364 column of Table 5. In order to compare values obtained with those derived from SVET
365 measurements it was assumed that mass loss was linear and an extrapolation made to assess
366 the mass loss over 24 hours. The calculated values are given in the fourth column of Table
367 5. The mass loss values measured by the gravimetric method and SVET were similar for

both the control and inhibited experiments as shown in Table 5. The efficiency of inhibition derived from physical mass loss experiments was 82 % and thus was again comparable to the SVET derived mass loss, providing validity of the SVET data at this solution pH.

(Table 5)

To further explore the inhibition at pH 2, SEM images were recorded for samples of Zn prior to immersion and post 24 hours immersion in pH 2 0.17 M NaCl with no inhibitor and the same solution containing 1 x 10^{-2} M L-tryptophan. These images are shown in Figure 11a, b and c respectively. Figure 11a, taken prior to electrolyte exposure, shows a distinct topography consistent with that created during sample preparation. Figure 11b demonstrates that significant corrosion has occurred on the Zn surface with no inhibitor present. In the case of 1 x 10^{-2} M L-tryptophan additions, Figure 11c, the surface does not demonstrate the level of corrosion and has a surface resembling that of the Zn prior to electrolyte exposure. This again provides support for the efficiency of L-tryptophan inhibition under these conditions, in line with the SVET and gravimetric mass loss data.

(Figure 11)

It would seem that at pH 2, polarization experiments do not provide an accurate assessment of the efficacy of L-tryptophan as a corrosion inhibitor when compared to the gravimetric data and subsequent support from SEM and SVET results. Thus, it may be conferred that the mechanism of action of the inhibitor is critically reliant on surface charge of the substrate and the ionic form of the L-tryptophan, as determined by the electrolyte pH, both of which may be altered through polarization.

4. Discussion

Inhibition via an adsorption mechanism; The exact nature of the inhibited surface has yet to be discerned. However, it is suggested that L-tryptophan offers initial protection to the zinc substrate via a film forming adsorption mechanism. At pH 7 this adsorption is observed optically in Figure 6b, which shows a uniform darkening of the zinc surface in the case that L-Tryptophan is present. Additionally, at the highest inhibitor concentration of 1 x 10^{-2} M there is a modification of the cathodic branch in the potentiodynamic data shown in Figure 3a where the zinc hydroxide reduction current peak, that was observed for the control experiment, is absent. This may indicate modification of the surface zinc hydroxide layer by the adsorbed species. Organic molecules adsorb by replacing water molecules, and thus the efficiency of the inhibitor is dependent on the electrostatic interaction between the metal and the inhibitor [36]. At pH 7 L-tryptophan exists in its zwitter ionic form. Furthermore, the zinc surface is predicted to be covered in zinc hydr (oxide) [31, 33], for which the isoelectric point is greater than pH 7 [37-39]. It thus follows that the surface is positively charged at this pH and that anionic L-tryptophan adsorbs directly onto the zinc surface, whilst the cationic form of L-tryptophan may adsorb via halide ions [40]. It has previously been found that halide ions adsorb on the metal surface by creating oriented dipoles and consequently increase the adsorption of the organic cations on the dipoles [41].

Due to the large dipole moment of a water molecule electrostatic bonding may not be strong enough, limiting inhibition efficiency [36]. The similarity of the potentiodynamic curves obtained in the absence and the presence of L-tryptophan is thus concurrent with findings regarding the potential dependent nature of L-tryptophan adsorption on metals [42]. However, there was a shift in OCP to cathodic potentials at pH 7 with an inhibitor concentration of 1 x 10^{-2} M, in addition to the absence of the hydroxide reduction peak in the cathodic branch of the potentiodynamic curve indicating that the inhibitor was interacting with the system

414 to a certain degree. It would therefore seem that the perturbation induced because of a
415 sweeping potential is disruptive to the inhibition mechanism that was observed in the
416 experiments conducted at OCP (SVET), and evidenced by the increase in R_p in the
417 inhibited systems at pH 7. At lower inhibitor concentrations insufficient surface film
418 coverage is provided, this being evidenced by the strong focal anode in the case of 1 x 10^{-3}
419 M additions and the similarity between the control and the electrolyte which contained 1
420 x 10^{-4} M L-tryptophan (Figure 4). At higher concentrations of 1 x 10^{-2} M L-tryptophan
421 sufficient surface coverage is initially achieved as evidenced by the low activity in Figure
422 4g, but it is probable that a breakdown of this protective 'film' may occur with respect to
423 time, a notion which is reinforced by the SVET results. Figure 4h shows the appearance of
424 an anode after 12 hours, after which the rate of zinc mass loss almost doubles. The internal
425 ring observed in the microscopy images, Figure 6b, is a corrosion product ring, similar to
426 that observed previously [20]. A breakdown in the protective film formed would allow
427 corrosion of the substrate to initiate, this resulting in the formation of the ring of corrosion
428 product.

429 At pH 11, the protonated amino group would lose its proton and the L-tryptophan would
430 behave as an anion. Moreover, in the case of Zn immersed in a pH 11 solution, E_{corr}- zcp,
431 where E_{corr} is the corrosion potential and zcp is the zero charge potential (the potential at
432 which there is no charge on the metal), is negative [36] and thus the surface is negatively
433 charged at the corrosion potential. Resultantly, L-tryptophan would initially be unable to
434 adsorb on the surface at this pH value due to the lack of electrostatic attraction, and thus
435 corrosion would proceed, this being supported by the presence of an anode both in Figure
436 8c and Figure 9b and the low inhibition efficiency calculated using R_p values measured
437 immediately after immersion (Table 2). In contrast to the microscopy images obtained in

438 the presence of L-Tryptophan at pH 7 (Figure 6b) uniform darkening does not occur at pH
439 11, supporting the notion that adsorption of L-tryptophan does not occur initially due to the
440 lack of electrostatic attraction between the negatively charged surface and the anionic
441 amino acid. The polarization curves in Figure 3b may support a mechanistic difference as
442 the suppression of the hydroxide reduction peak on the cathodic branch is not observed at
443 pH 11, as was the case at pH 7.

444 Below pH 2.38 the net charge of L-tryptophan is positive as the carboxyl group is
445 protonated [14]. Moreover, in the case of Zn in an acidic solution, E_{corr}- zcp is positive [36] and
446 thus the surface is positively charged at the corrosion potential. Inhibitors have previously
447 been found to work best in halide containing solutions as the positive charge they carry is
448 neutralized by the halide ion, leading to stronger adsorption at the interface [40]. This
449 synergistic effect of halide ions has been investigated previously. Lorenz concluded that
450 halide ions adsorb on the metal surface by creating oriented dipoles and consequently
451 increase the adsorption of the organic cations on the dipoles [41]. It is thus proposed that in
452 pH 2 electrolyte adsorption of the protonated L-tryptophan occurs via Cl^- at the positive
453 zinc surface, this mechanism being suggested elsewhere in the case of steel [12]. It would
454 seem that this mechanism provides suitable coverage of the substrate surface given the 82-
455 88 % inhibition efficiency and reduction in surface damage demonstrated at pH 2.

456 ***Inhibition via formation of an insoluble zinc-Tryptophan complex***

457 In addition to the adsorption mechanism proposed to offer inhibition through film
458 formation, a secondary protection mechanism, whereby a species is formed as a result of
459 local pH changes adjacent to anodic regions, is also a possibility. In basic conditions, above
460 pKa_2=9.38, the protonated amino groups of the L-tryptophan loses its proton, via equation

(2), to give the anionic form of L-tryptophan, L^- [14]. This anion can react with metal ions to form mono, bis and tris complexes. Zn^{2+} ions formed can therefore migrate towards areas of cathodic activity whereby they combine with the anions to form a film, reducing the corrosion activity of the surface in this region. This process may be shown in Figure 5 where regions of cathodic activity on the Zn surface are de-activated with respect to time with a subsequent decrease in anodic activity as demonstrated in the in-set figure.

The formation of a double complex of minimum solubility with the deprotonated ligand, equation (6) with formation constant, β, is proposed according to equation (7)

$$Zn^{2+} + L^- \rightarrow (ZnL)^- \quad (6)$$

$$\beta = \frac{1}{k_{diss}} = \frac{[ZnL]^-}{[Zn^{2+}]\,[L^-]} \quad (7)$$

Values of log β for the mono, bi and tri complexes have previously been given as 5.01-5.21, 8.2-9.89 and 13.50 respectively [43]. A poorly soluble complex between divalent Zn (II) and L-tryptophan has also been found to form elsewhere [44]. Amongst the selected amino acids tested (tyrosine, cysteine, histidine and alanine), the most stable complexes were those formed by Zn (II) in combination with L-tryptophan, for which the stability constant was determined to be (405.78 ± 12.17) μM^{-1} [44].

At pH 11, where the presence of L-tryptophan was initially observed to have little effect on corrosion, the formation of this insoluble product proximal to the site of cation release, means that little activity is observed after 8 hours of immersion (Figure 8d). This reduction in SVET derived zinc mass loss correlates with a decrease in corrosion potential (Figure 2b), which is indicative of a decrease in cathodic activity, as well as an increase in R_p (Table 2). There is significant precipitation of product more proximal to developing corrosion sites

(Figure 9b) and this would support the inhibition mechanism proposed with respect to the formation of complex between anionic L-tryptophan with metal ions released into solution.

The increased reduction in mass loss, and thus inhibition efficiency of 80%, observed in the case pH 11 electrolytes, when compared to pH 7, 64%, are suggested to be a result of the increased NH_2/NH_3^+ ratio, as calculated using the Henderson-Hasselbalch equation (8)

$$pH = pK_a + \log\frac{[A^-]}{[HA]} \quad (8)$$

At pH 11 there will be a 40:1 ratio as opposed to the 1:245 ratio at pH 7. Resultantly more L-tryptophan will exist in the anionic form at this higher pH, thus allowing greater precipitation of insoluble Zn tryptophan species.

A 1 unit change in pH over 24 hours, consistent with previous findings was observed in the case of pH 11 electrolytes [45]. The resultant decrease in the NH_2/NH^{3+} ratio would, following the above argument, lead to a decreased inhibition efficiency with time. In contrast, the corrosion rate was constant throughout the experimental time period in the absence of L-tryptophan, and decreased over time in the presence of L-tryptophan. It is therefore believed that the variation in pH was not the primary cause of any change in corrosion rate.

The exact nature of the inhibitive film is not yet fully understood, and, given the effectiveness of L-tryptophan, especially at pH 2, should be the subject of further work. The stability of the inhibitive effect is also an area of future research, this being especially true when considering changes in electrolyte pH over the 24 hour experimental period, as discussed previously.

5. Conclusions

A systematic optical and electrochemical study has been completed to investigate the influence of the amino acid, L-tryptophan, on the localized corrosion occurring on unpolarized zinc (Zn) samples immersed in a 0.17 M aqueous sodium chloride electrolyte at various values of pH. The onset of significant corrosion inhibition was achieved at a threshold concentration of 1 x 10^{-2} M L-Tryptophan additions at all pH levels. At pH 2 the additions resulted in an 88 % decrease in mass loss, as measured by gravimetric mass loss results and SVET, demonstrating the potential of L-tryptophan inhibitors for this material within acidic environments. Lower inhibition efficiencies of 80 % and 64 % were observed at pH 11 and pH 7 respectively, as derived from SVET mass loss measurements. An inhibition mechanism is proposed whereby L-Tryptophan is adsorbed onto the Zn surface as observed through in-situ time lapse microscopy experiments. At pH 2 adsorption of the protonated L-tryptophan may occur via Cl^-. At pH 7 adsorption of the zwitter ion form of L-Tryptophan may be directly to the metal surface or via Cl^- ions. The formation of a protective complex between Zn^{2+} and anionic L-Tryptophan due to a local increase in pH is also a possibility. This has been evidenced by mechanistic changes observed at pH 11 through time lapse microscopy whereby precipitation of a product is observed coincident with localized corrosion sites. The results demonstrate the potential use of the amino acid L-tryptophan as an environmentally friendly corrosion inhibitor on Zn, but highlight the significant effect of pH on the efficiency of inhibition.

5. Acknowledgments

The authors would like to thank the College of Engineering (Swansea University) for their support. Dr. J.D. McGettrick is gratefully acknowledged for acquiring the XPS data.

6. Tables

528 Table 1. Free corrosion potential of pure zinc in 0.17 M NaCl containing various
529 concentrations of L-tryptophan at 25 °C.

pH	L Tryptophan concentration (M)	E_{corr} (vs. SHE)
7	0	-0.868 ± 0.02
	10^{-4}	-0.863 ± 0.01
	10^{-3}	-0.874 ± 0.004
	10^{-2}	-0.903 ± 0.009
2	0	-0.846 ± 0.02
	10^{-2}	-0.836 ± 0.002
11	0	-0.866 ± 0.004
	10^{-2}	-1.011 ± 0.002

530 Table 2. Calculated polarization resistance (R_p) and inhibitor efficiency values for a pure
531 zinc sample freely corroding in pH 7 and pH 11, 0.17 M NaCl (aq) electrolyte in the
532 absence and presence of L-tryptophan additions as a function of time.

pH	Time (hours)	R_{p0} (Ohms.cm^2)	R_{pi} (Ohms.cm^2)	Inhibition Efficiency (%)
7	0	304	1380	78
	6	448	2130	79
	12	428	2520	83
11	0	2220	1195	0
	6	1240	1652	25
	12	573	1622	65

533 Table 3. SVET derived mass loss calculated for a zinc sample freely corroding in pH 7 0.17
534 M NaCl (aq) electrolyte with varying L-tryptophan additions, for 24 hours.

L Tryptophan concentration (M)	Mass loss (g.m^{-2})	Inhibition Efficiency (%)
0	3.65 ± 0.60	
10^{-4}	3.41 ± 0.56	7
10^{-3}	4.01 ± 0.66	0
10^{-2}	1.32 ± 0.24	64

535 Table 4. SVET derived mass loss values calculated for a pure zinc sample freely corroding
536 in pH 2, pH 7 and pH 11, 0.17 M NaCl (aq) electrolyte with 0 and 10^{-2} M L-tryptophan
537 additions for 24 hours.

pH	L Tryptophan concentration (M)	Mass loss (g.m^{-2})	Inhibition Efficiency (%)
7	0	3.65 ± 0.60	
	10^{-2}	1.32 ± 0.24	64
2	0	17.96 ± 2.95	
	10^{-2}	2.03 ± 0.33	88
11	0	4.43 ± 0.73	

	10^{-2}	0.90 ± 0.15	80

Table 5. SVET derived and physical mass loss values calculated for a pure zinc sample freely corroding in pH 2 0.17 M NaCl (aq) electrolyte with 0 and 10^{-2} M L-tryptophan additions.

Technique	**L Tryptophan concentration (M)**	**Measured Mass Loss over 7 days (mg)**	**Normalised Mass loss ($g.m^{-2}$)**	**Inhibition Efficiency (%)**
SVET	0		17.96 ± 2.95	
	10^{-2}		2.03 ± 0.33	88
Gravimetric	0	280 ± 40	16.00 ± 2.29	
	10^{-2}	51 ± 7	2.91 ± 0.40	82

7. Figure Legends

Figure 1. Molecular structure of L-tryptophan

Figure 2. Free Corrosion Potential of pure zinc in a.) pH 7 b.) pH 11 and c.) pH 2, 0.17 M NaCl (aq) electrolyte with i.) _____ 0 ii.) _____ 10^{-2} M iii.) _____ 10^{-3} M and iv.) _____ 10^{-4} M L-Tryptophan additions.

Figure 3. Current density as a function of potential for pure zinc in a.) pH 7 b.) pH 11 and c.) pH 2 0.17 M NaCl (aq) electrolyte with i.) _____ 0 ii.) _____ 10^{-2} M iii.) _____ 10^{-3} M and iv.) _____ 10^{-4} M L-Tryptophan additions.

Figure 4. SVET derived surface plots maps showing the distribution of normal current density J_z above a zinc sample freely corroding in pH 7 0.17 M NaCl (aq) electrolyte with a-b.) 0, c-d.) 10^{-4} M, e-f.) 10^{-3} M, g-h.) 10^{-2} M L-tryptophan additions after various times of immersion.

Figure 5. a.) An SVET derived surface plot map indicating the region from which normal current density J_z values for b.) were taken and b.) Profile showing normal current density J_z as a function of distance away from the focal anodic site taken above a zinc sample freely corroding in pH 7 0.17 M NaCl (aq) electrolyte with 10^{-3} M L-tryptophan additions at 8 hour intervals. Initial time 8 hours. Inset, profile showing extended current density range. Arrow 1 shows a decrease in anodic activity with time, arrow 2 shows a decrease in anodic activity with time and arrow 3 shows an extension in the region of low activity.

Figure 6. Optical microscope images of zinc taken in situ under immersion conditions in pH 7 0.17 M NaCl (aq) electrolyte with a.) 0 b.) 10^{-2} M L-Tryptophan additions. Images shown were taken at hour intervals.

Figure 7. XPS spectra, with fitted nitrogen curves, from the outermost surface of zinc sample immersed in pH 7 0.17 M NaCl (aq) with i.) _____ 0 ii.) __ . . __ . . 10^{-2} M L-tryptophan additions.

Figure 8. SVET derived surface plots maps showing the distribution of normal current density J_z above a zinc sample freely corroding in pH 11 0.17 M NaCl (aq) electrolyte with a-b.) 0, c-d.) 10^{-2} M L-tryptophan additions.

Figure 9. Optical microscope images of zinc taken in situ under immersion conditions in pH 11 0.17 M NaCl (aq) electrolyte with a.) 0 b.) 10^{-2} M L-Tryptophan additions. Images shown were taken at 30 minute intervals.

Figure 10. SVET derived surface plots maps showing the distribution of normal current density J_z above a zinc sample freely corroding in pH 2 0.17 M NaCl (aq) electrolyte with a-b.) 0, c-d.) 10^{-2} M L-tryptophan additions.

Figure 11. An SEM image of the zinc surface a.) prior to electrolyte exposure b.) after immersion in pH 2, 0.17 M NaCl (aq) electrolyte and c.) after immersion in pH 2, 0.17 M NaCl (aq) electrolyte with 10^{-2} M L-tryptophan additions, for 24 hours.

7. References

1. A. Pilbáth, L. Nyikos, I. Bertóti, E. Kálmán, Corrosion Science, **50**, 3314 (2008).
2. K. Aramaki, Corrosion Science, **43**, 1985 (2001).
3. S. Manov, A. Lamazouère, L. Ariès, Corrosion Science, **42**, 1235 (2000).
4. F. Suedile, F. Robert, C. Roos, M. Lebrini, Electrochimica Acta, **133**, 631 (2014).
5. I. A. Kartsonakis, S. G. Stanciu, A. A. Matei, R. Hristu, A. Karantonis, C. A. Charitidis, Corrosion Science, **112**, 289 (2016).
6. M.A. Deyab, Journal of Power Sources, **292**, 66 (2015).
7. S. Liu, Y. Zhong, R. Jiang, Z. Zeng, Z. Feng, R. Xiao, Corrosion Science, **53**, 746 (2011).
8. S. A. Umoren, M. M. Solomon, Journal of Environmental Chemical Engineering, **5**, 246 (2017).
9. V. Shkirskiy, P. Keil, H. Hintze-Bruening, F. Leroux, F. Brisset, K. Ogle, P. Volovitch, Corrosion Science, **100**, 101 (2015).
10. H. Nady, Tricine [N-(Tri(hydroxymethyl)methyl)glycine] – A novel green inhibitor for the corrosion inhibition of zinc in neutral sodium chloride solutions, Egyptian Journal of Petroleum (2016), http://dx.doi.org/10.1016/j.ejpe.2016.02.004.
11. H. Ashassi-Sorkhabi, Z. Ghasemi, D. Seifzadeh, Applied Surface Science, **249**, 408 (2005).

12. J.-J. Fu, S.-N. Li, L.-H. Cao, Y. Wang, L.-H. Y, L.-D. Lu, J. Mater. Sci., **45**, 979 (2010).

13. G. Moretti, F. Guidi, Corrosion Science, **44**, 1995 (2002).

14. R. M. C. Dawson, *Data for Biochemical Research*, Clarendon Press (1969).

15. G. Williams, H. N. Mcmurray, R. Grace, Electrochimica Acta, **55**, 7824 (2010).

16. J. Elvins, J. A. Spittle, D. A. Worsley, Corrosion Science, **47**, 2740 (2005).

17. J. Sullivan, C. Weirman, J. Kennedy, D. J. Penney, Corrosion Science, **52**, 1853 (2010).

18. D. J. Penney, J. H. Sullivan, D. A. Worsley, Corrosion Science, **49**, 1321 (2007).

19. J. Elvins, J. A. Spittle, J. H. Sullivan, D. A. Worsley, Corrosion Science, **50**, 1650 (2008).

20. J. Sullivan, N. Cooze, C. Gallagher, T. Lewis, T. Prosek, D. Thierry, Faraday Discussions, **180**, 361 (2015).

21. T. Prosek, J. Hagstöm, D. Persson, N. Fuertes, F. Linberg, O. Chocholatý, C. Taxén, J. Šerák, D. Thierry, Corrosion Science, **110**, 71 (2016).

22. T. Prosek, D. Thierry, C. Taxén, J. Maixner, Corrosion Science, **49**, 2676 (2007).

23. G. Williams, H. N. McMurray, Journal of the Electrochemical Society, **155**, C340 (2008).

24. S. Bohm, H.N. McMurray, S.M. Powell, D.A. Worsley, Electrochimica Acta, **45**, 2165 (2000).

25. D. Worsley, H. N. McMurray, A. Belghazi, Chem. Commun., 2369 (1997).

26. S. M. Powell, D. A. Worsley, Br. Corrosion J., **36**, 42 (2001).

27. G.W.C. Kaye, T.H. Laby, *Tables of Physical and Chemical Constants*, p. 219, Longman, London (1986).

28. D.A. Worsley, H.N. McMurray, J.H. Sullivan, I.P. Williams, Corrosion, **60**, 437 (2004).

29. A.C. Bastos, M.L. Zheludkevich, M.G.S. Ferreira, Portugaliae Electrochimica Acta, **26**, 47 (2008).

30. J. H. Sullivan, S. Mehraban, J. Elvins, Corrosion Science, **53**, 2208 (2011).

31. S. Thomas, N. Birbilis, M.S. Venkatraman, I.S. Cole, Corrosion, **68**, 015009-1 (2012).

32. H. Dafydd, D.A. Worsley, H.N. McMurray, Corrosion Science, **47**, 3006 (2005).

33. M. Pourbaix, *Atlas of Electrochemical Equilibria in Aqueous Solutions*, Pergamon Press (1966).

34. W. Miao, I. S. Cole, A. K. Neufeld, S. Furman, Journal of the Electrochemical Society, **154**, C7 (2007).

35. X. G. Zhang, *Corrosion and Electrochemistry of Zinc*, Springer Science & Business Media (1996).

36. S. Papavinasam Corrosion Inhibitors, in *Uhlig's Corrosion Handbook*, 3rd Edition ed R. W. Revie, p. 1089, John Wiley & Sons, Inc., Hoboken, NJ, USA (2011).

37. R. Marsalek, APCBEE Procedia, **9**, 13 (2014).

38. K. Jurkiewicz, International Journal of Mineral Processi*ng*, **29**, 1 (1990).

39. G. Redmond, A. O'Keeffe, C. Burgess, C. MacHale, D. Fitzmaurice, The Journal of Physical Chemistry, **97**, 11081 (1993).

40. J. O'M. Bockris, B. Yang, Journal of the Electrochemical Society, **138**, 2237 (1991).

41. Lorenz, W.J, Z. Phys. Chem., **65**, 244 (1970).

42. J.B. Craig, C. J. Mackay, Journal of Materials Science: Materials in Medicine, **7**, 567 (1996).

43. L. D. Pettit. Pure Appl. Chem., **56**, 247 (1984).

44. B. Dolińska, Il Farmaco, **56**, 737 (2001).

45. T. N. Vu, P. Volovitch, K. Ogle, Corrosion Science, **67,** 42 **(2013).**

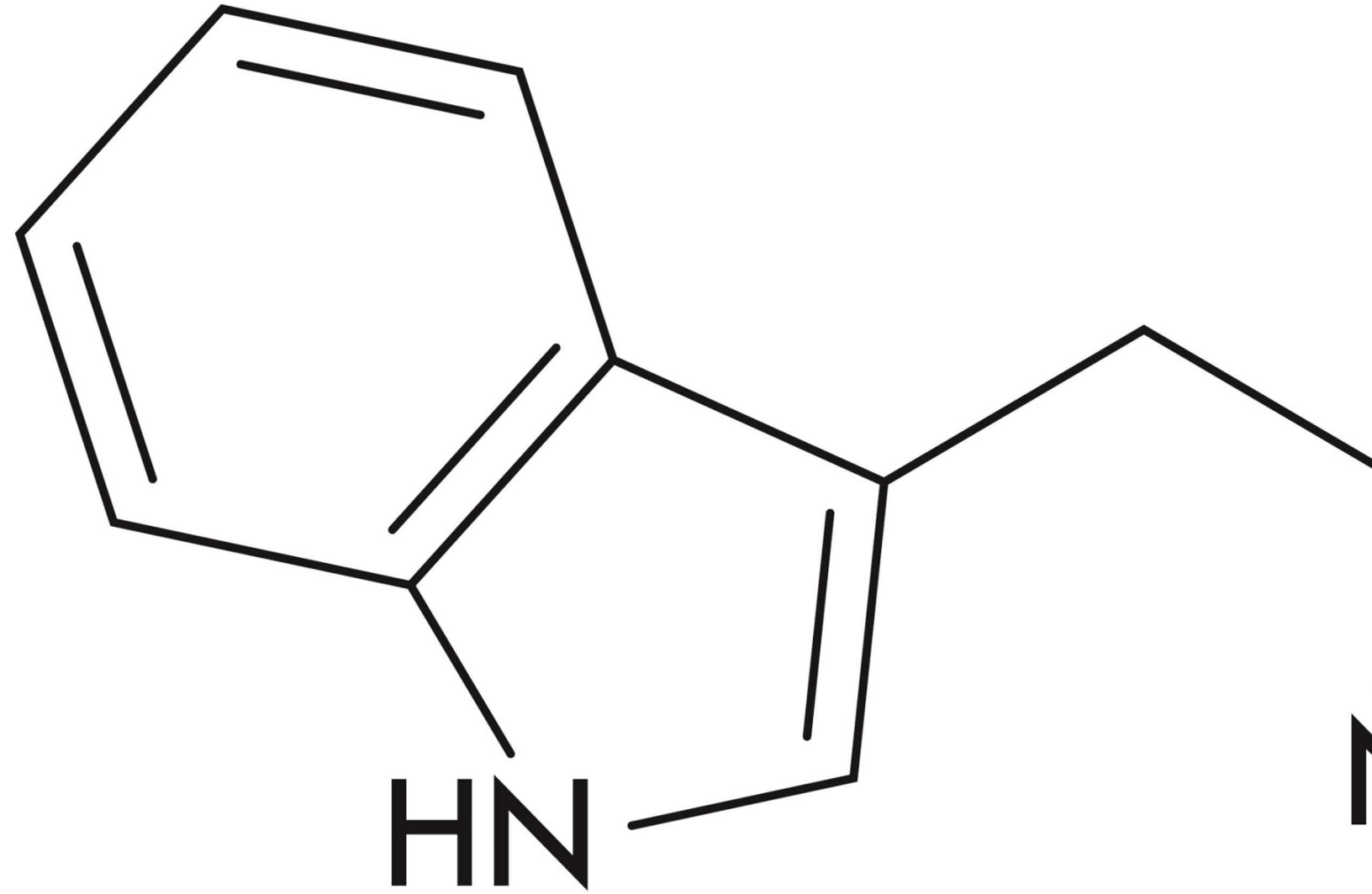
HN

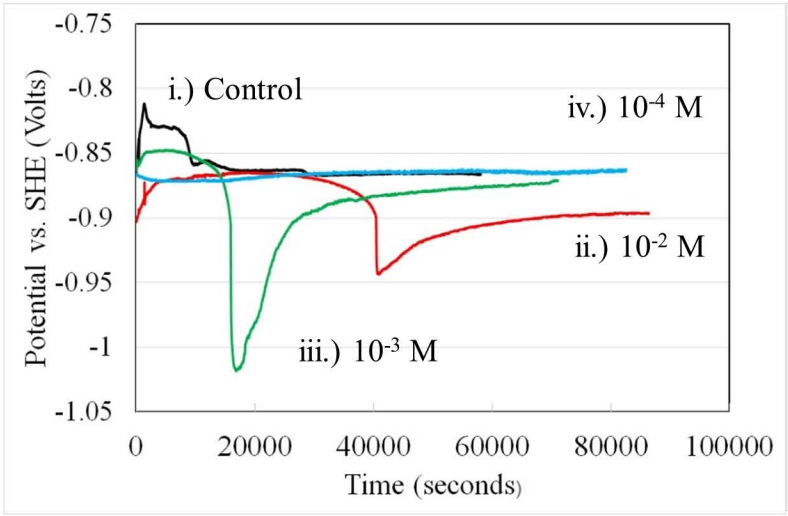
-0.75
-0.8
-0.85
-0.9
-0.95
-1
-1.05
Potential vs. SHE (Volts)
i.) Control
iv.) 10-4 M
ii.) 10-2 M
iii.) 10-3 M
0
20000
40000
60000
80000
100000
Time (seconds)

a.)

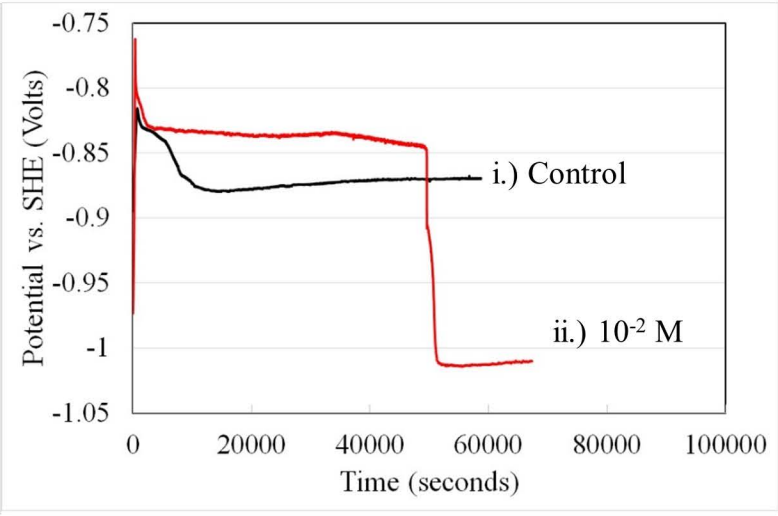
-0.75
-0.8
-0.85
-0.9
-0.95
-1
-1.05
Potential vs. SHE (Volts)
i.) Control
ii.) 10-2 M
0
20000
40000
60000
80000
100000
Time (seconds)

b.)

c.

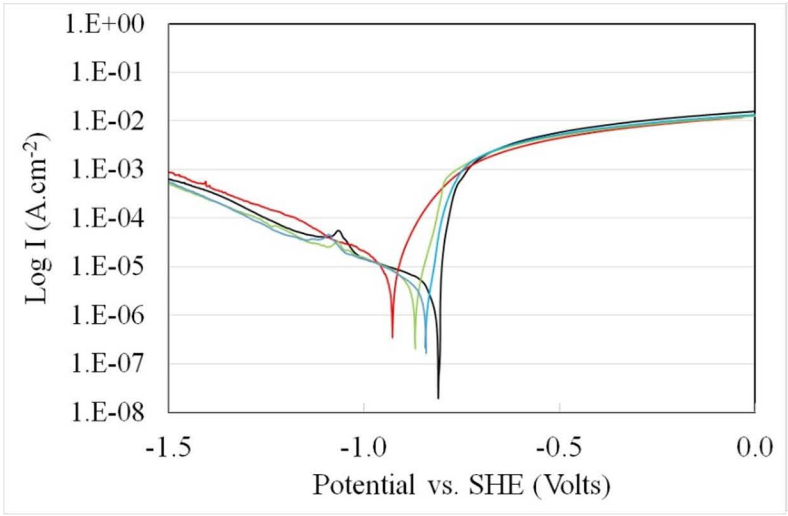
1.E+00
1.E-01
1.E-02
1.E-03
1.E-04
1.E-05
1.E-06
1.E-07
1.E-08
Log I (A.cm-2)
-1.5
-1.0
-0.5
0.0
Potential vs. SHE (Volts)

a.)

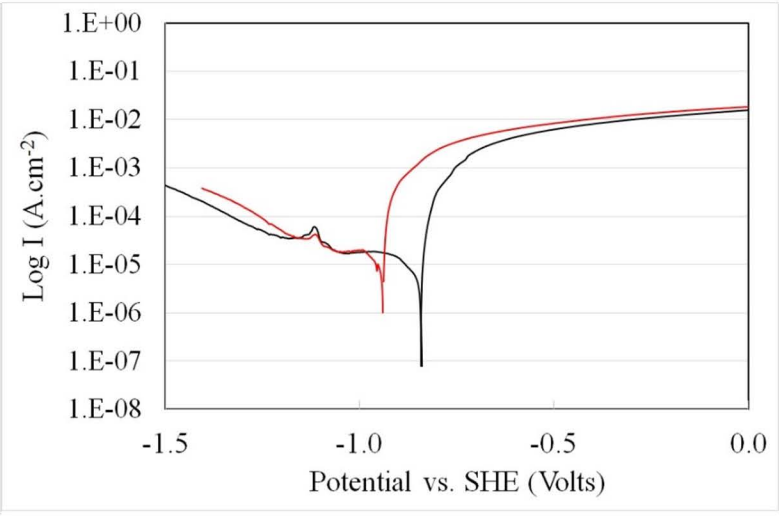
1.E+00
1.E-01
1.E-02
1.E-03
1.E-04
1.E-05
1.E-06
1.E-07
1.E-08
Log I (A.cm-2)
-1.5
-1.0
-0.5
0.0
Potential vs. SHE (Volts)

b.)

c.

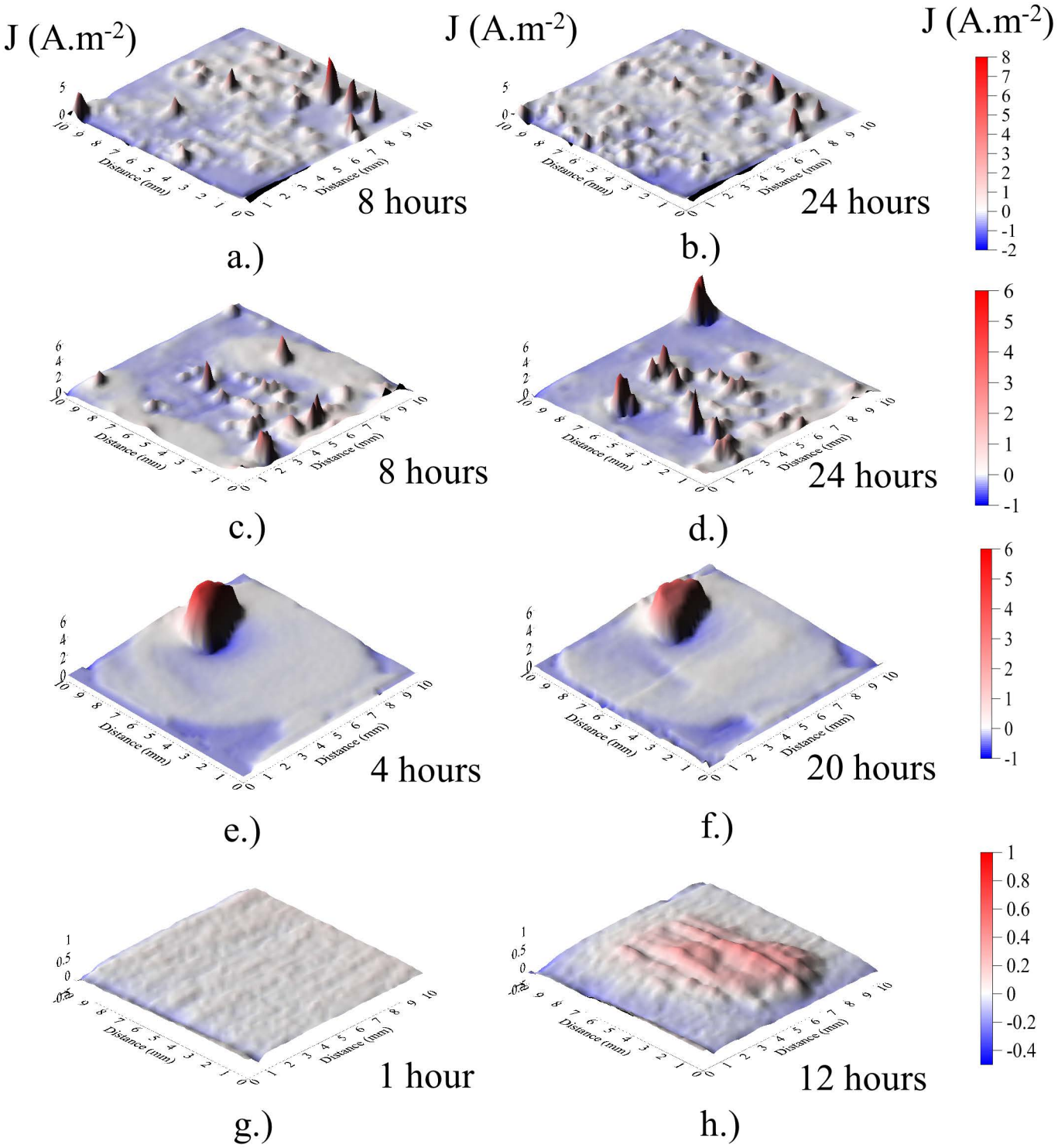
J (A.m-2)
J (A.m-2)
J (A.m-2)
Distance (mm)
Distance (mm)
8 hours
24 hours
a.)
b.)
8 hours
24 hours
c.)
d.)
4 hours
20 hours
e.)
f.)
1 hour
12 hours
g.)
h.)

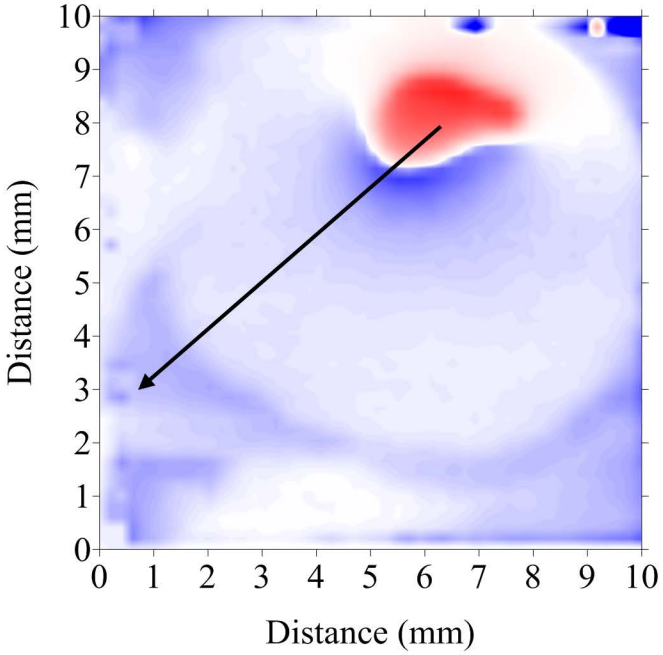
Distance (mm)
Distance (mm)
0
1
2
3
4
5
6
7
8
9
10

a.)

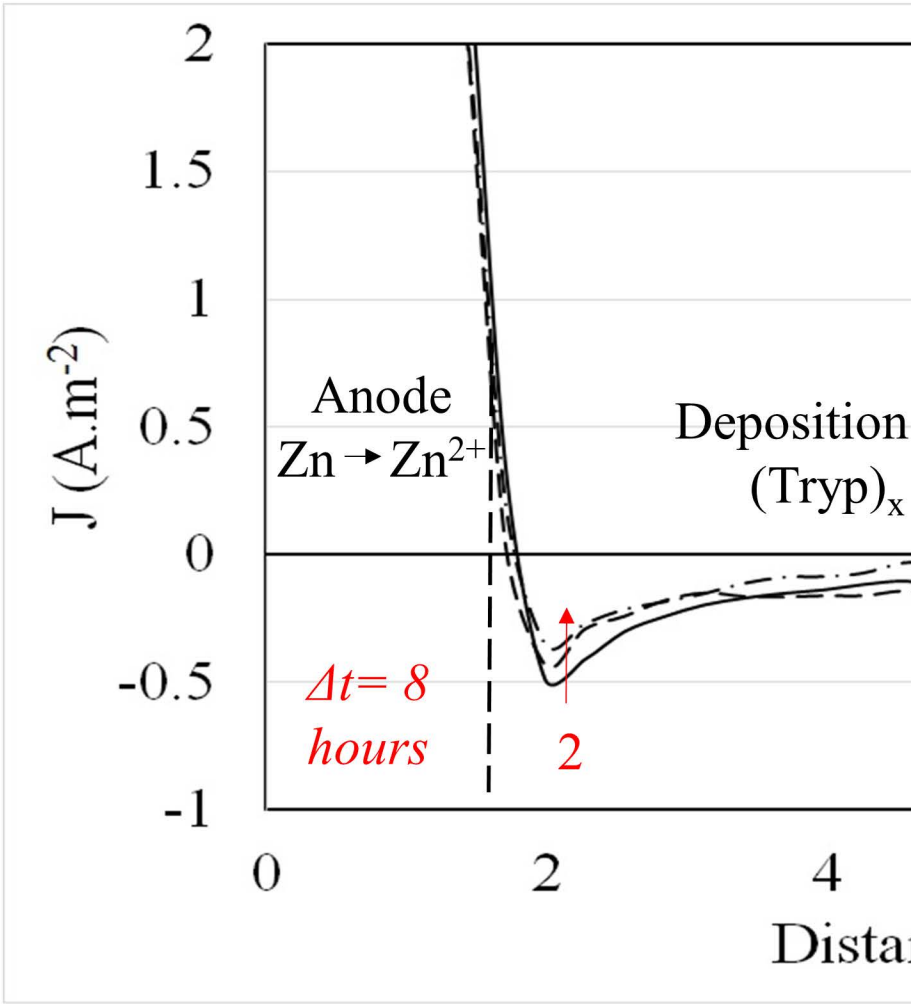
J (A.m-2)
2
1.5
1
0.5
0
-0.5
-1
Anode
Zn → Zn2+
Deposition
(Tryp)x
Δt= 8
hours
2
0
2
4

b

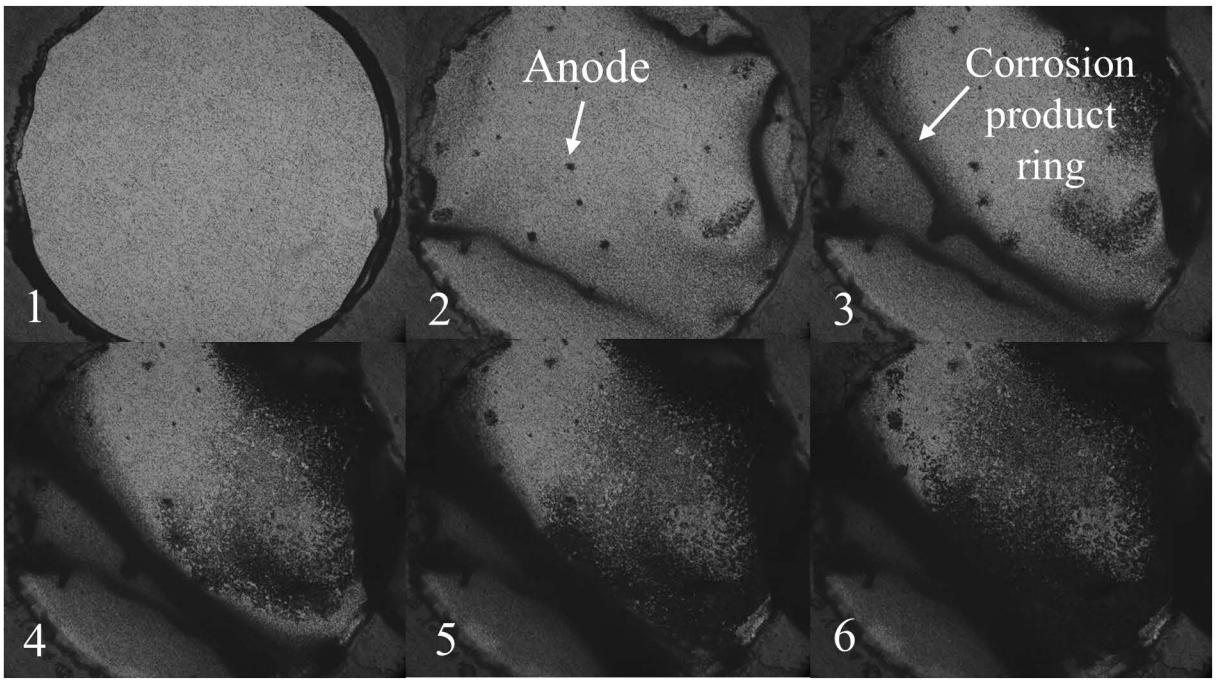

a.) —— 200µm

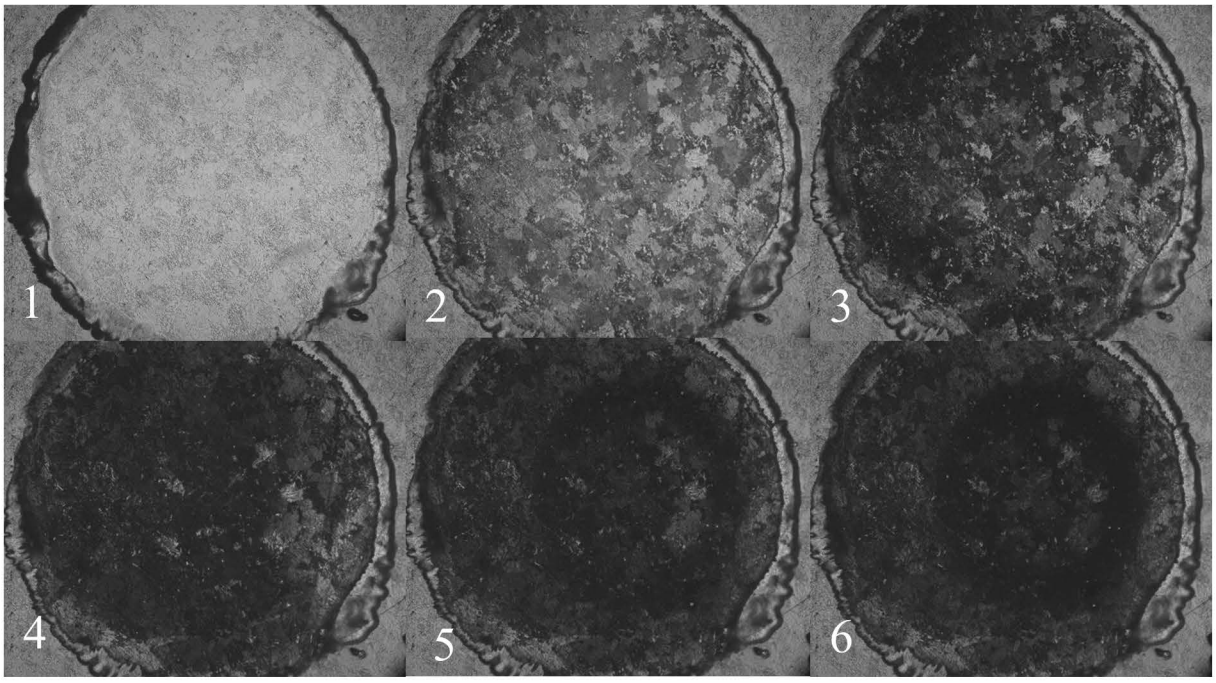

b.)

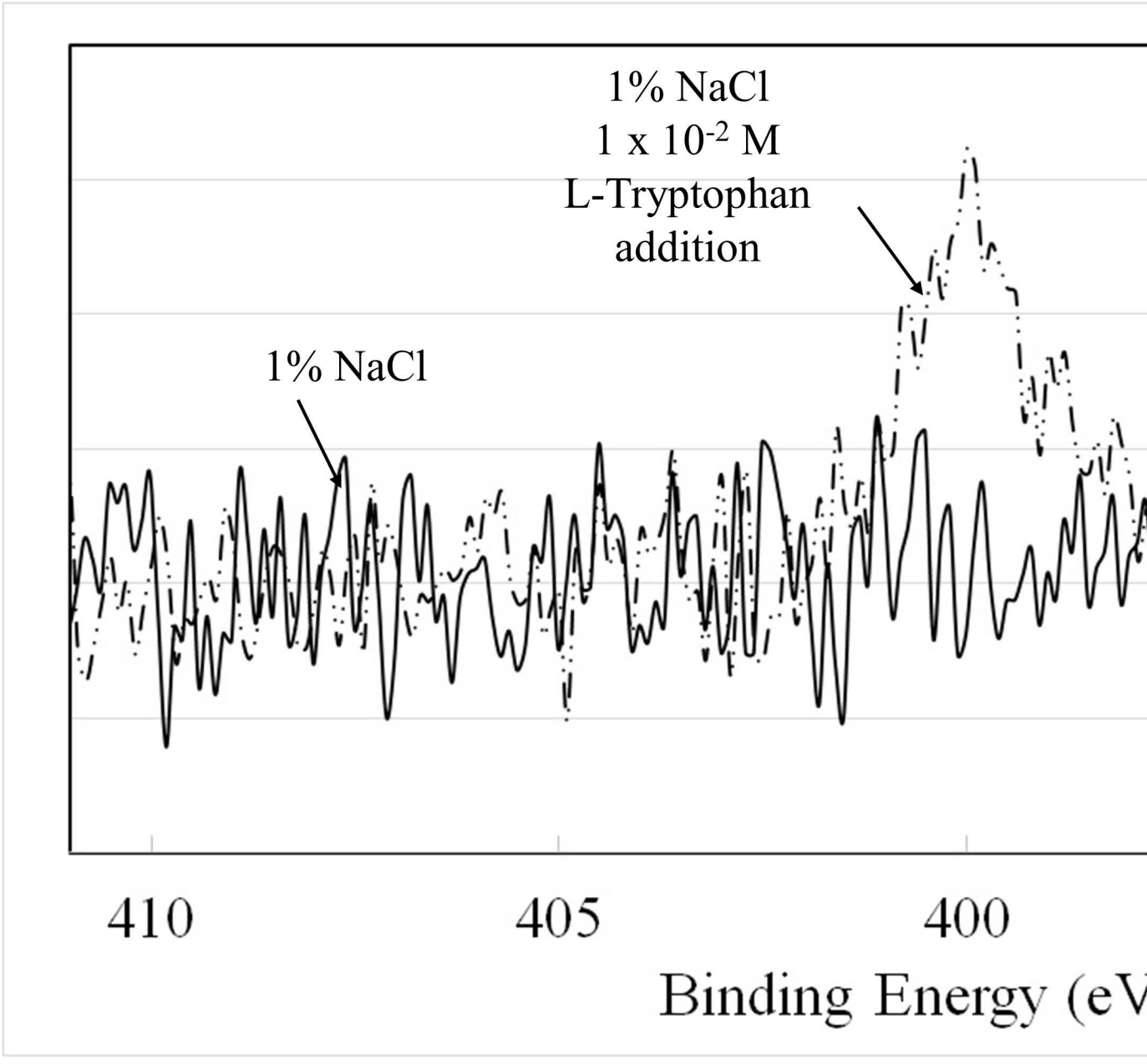
1% NaCl
1 x 10-2 M
L-Tryptophan
addition
1% NaCl
410
405
400
Binding Energy (eV

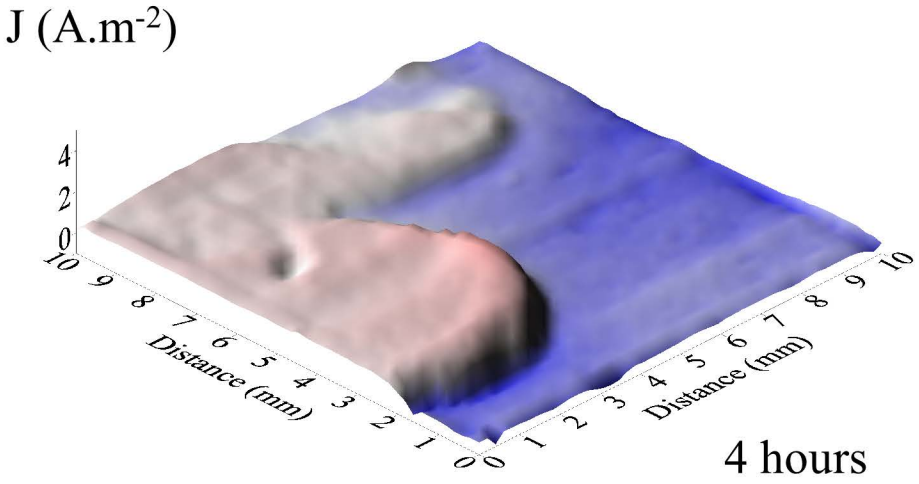
J (A.m-2)
4
2
0
10 9 8 7 6 5 4 3 2 1 0
Distance (mm)
0 1 2 3 4 5 6 7 8 9 10
Distance (mm)
4 hours

a.)

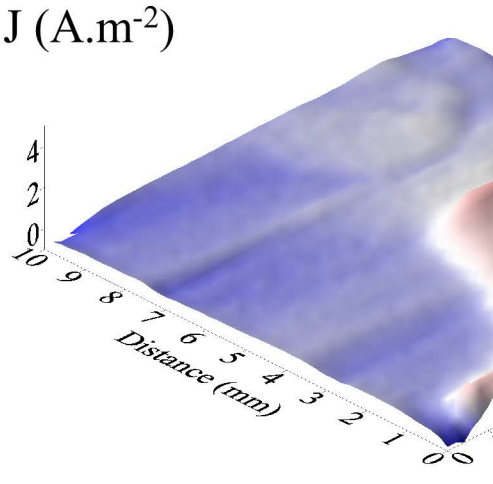
J (A.m-2)
4
2
0
10 9 8 7 6 5 4 3 2 1 0
Distance (mm)

b.)

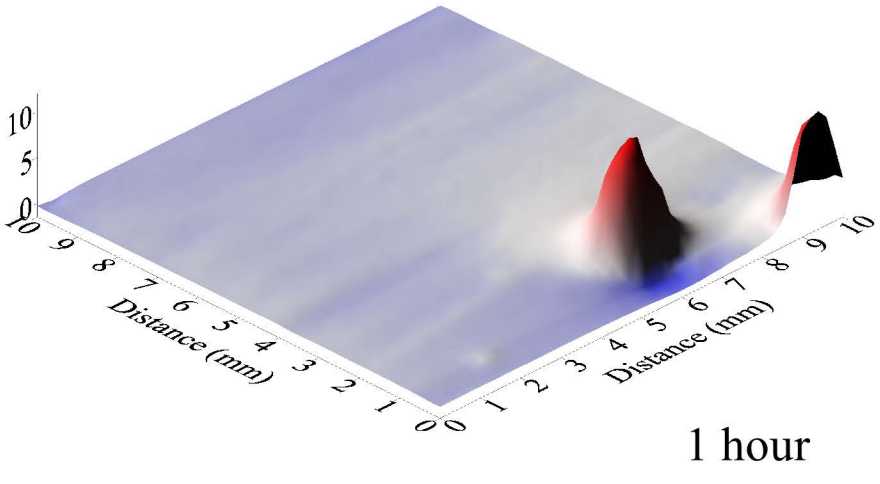
10
5
0
10 9 8 7 6 5 4 3 2 1 0
Distance (mm)
0 1 2 3 4 5 6 7 8 9 10
Distance (mm)
1 hour

c.)

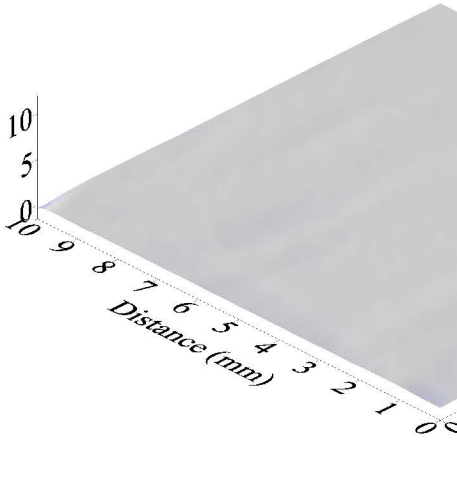
10
5
0
10 9 8 7 6 5 4 3 2 1 0
Distance (mm)

d.)

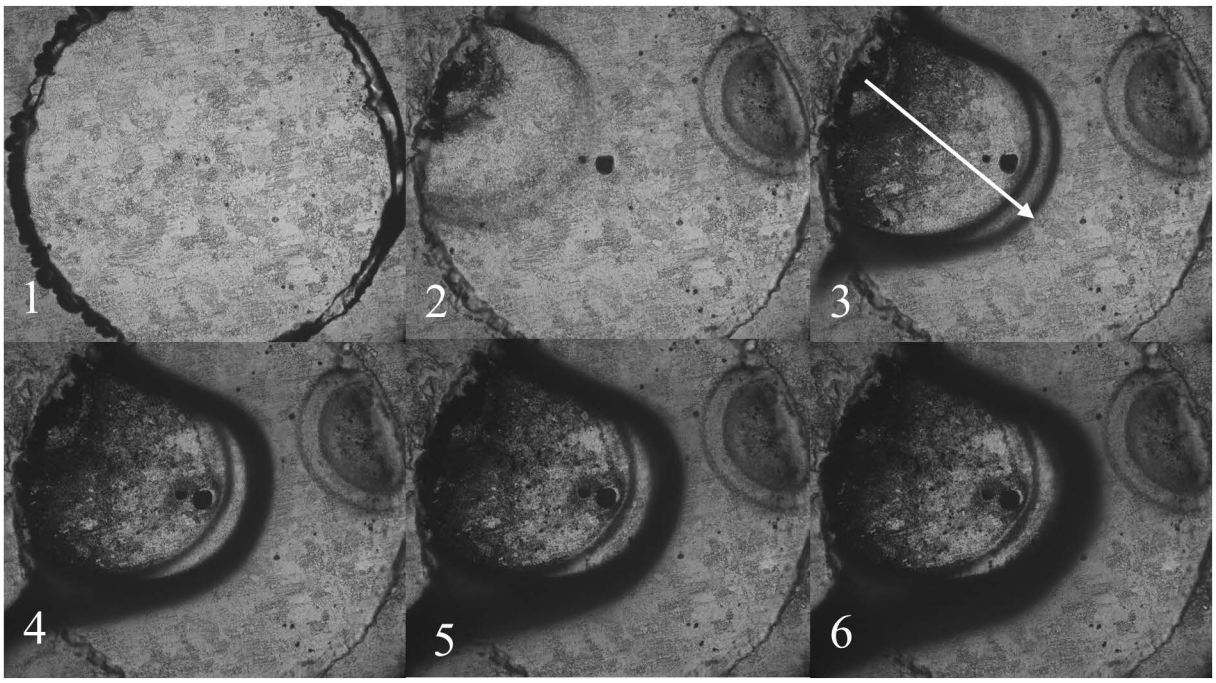

a.)

200µm

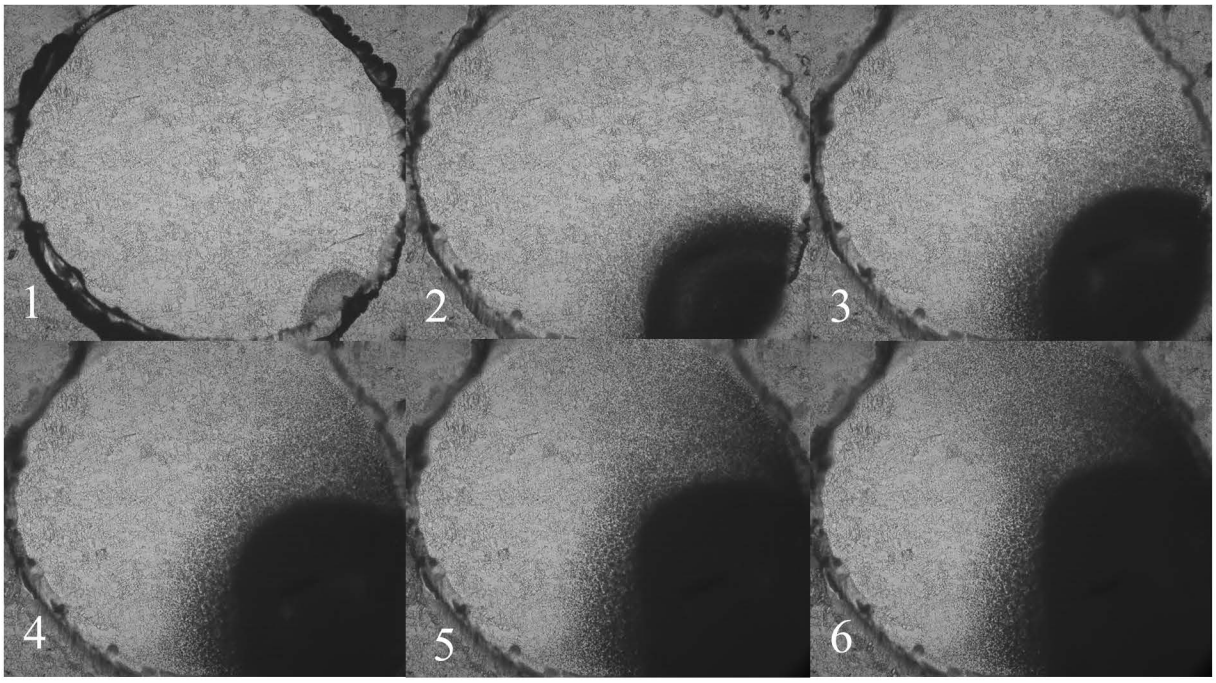

b.)

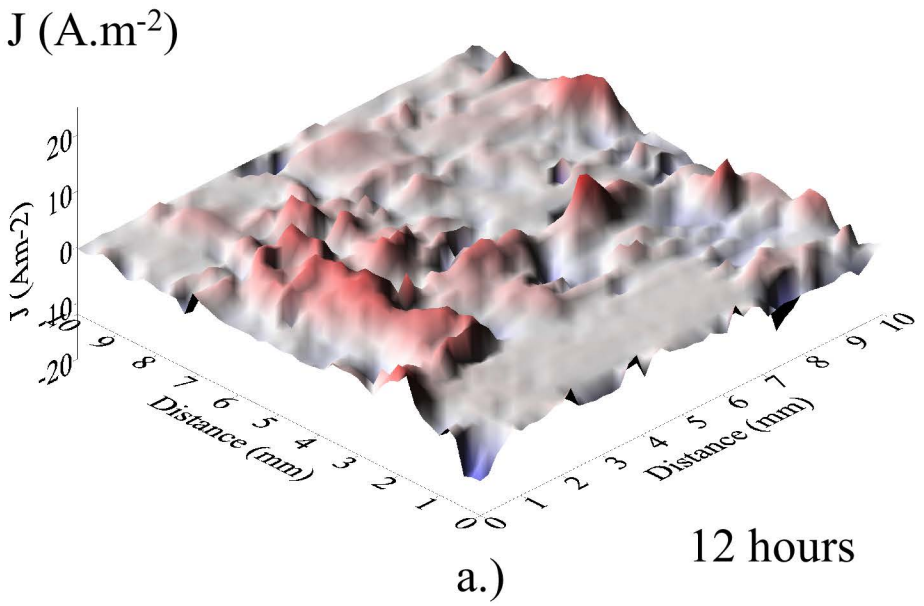
J (A.m-2)
J (Am-2)
20
10
0
-10
-20
Distance (mm)
Distance (mm)
12 hours

a.)

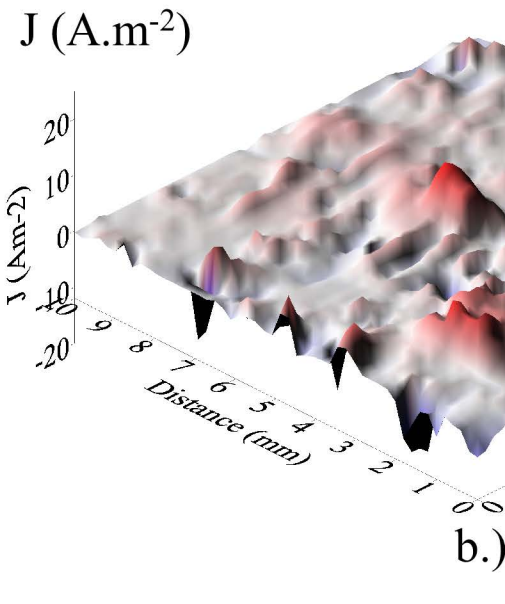
J (A.m-2)
J (Am-2)
20
10
0
-10
-20
Distance (mm)

b.)

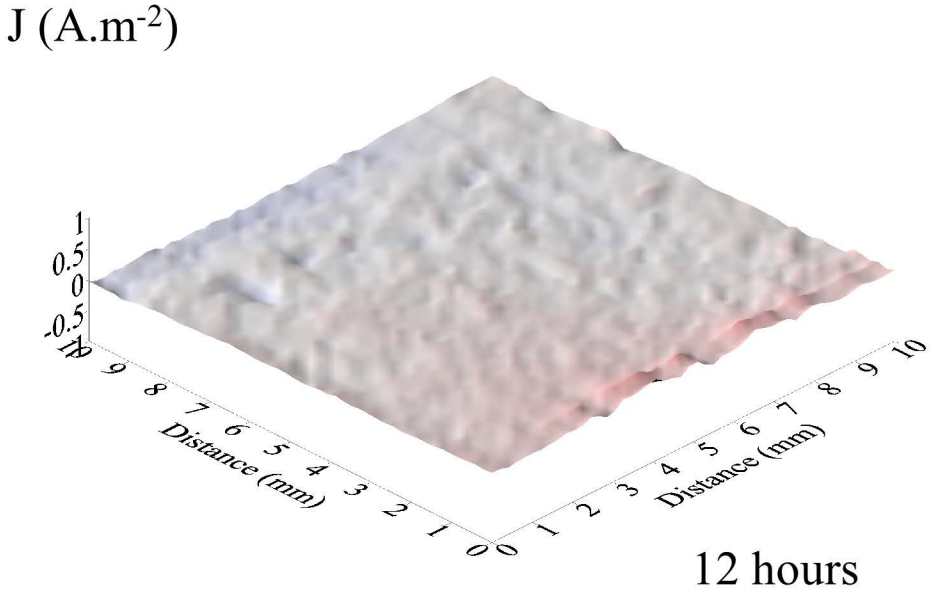
J (A.m-2)
1
0.5
0
-0.5
-1
Distance (mm)
Distance (mm)
12 hours

c.)

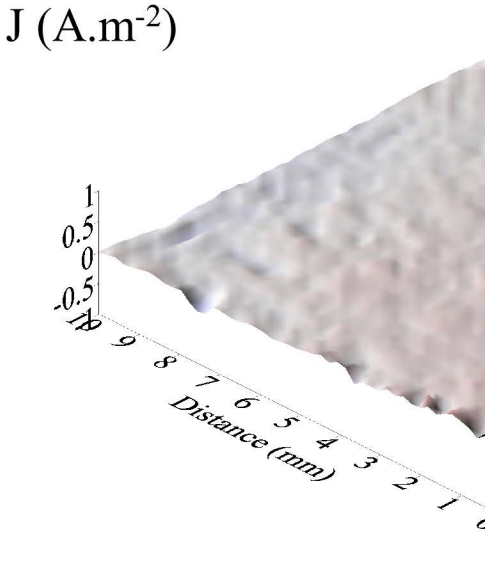
J (A.m-2)
1
0.5
0
-0.5
-1
Distance (mm)

a.)

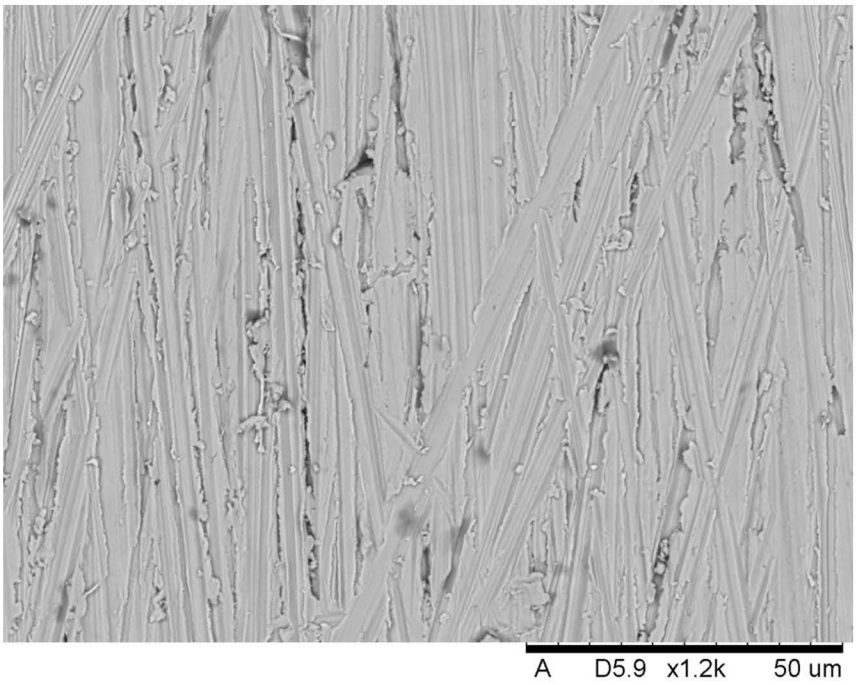

b.)

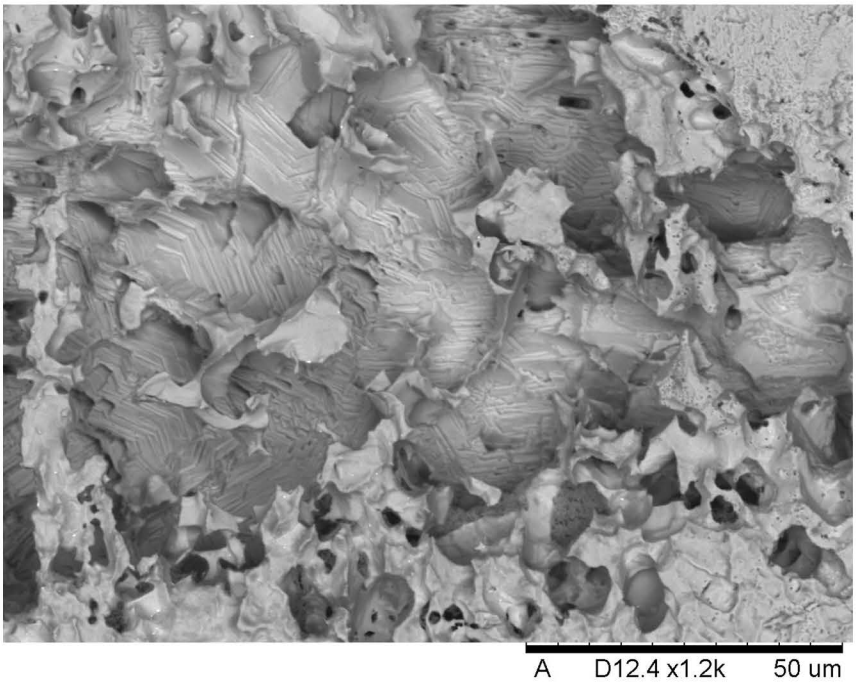

c.)